Available online at www.sciencedirect.com
ScienceDirect
Planetary and Space Science 55 (2007) 1398–1413
Planetary and Space Science
www.elsevier.com/locate/pss

The BepiColombo Laser Altimeter (BELA): Concept and baseline design

N. Thomas[a,*], T. Spohn[b], J.-P. Barriot[c], W. Benz[a], G. Beutler[d], U. Christensen[e], V. Dehant[f], C. Fallnich[g], D. Giardini[h], O. Groussin[i], K. Gunderson[a], E. Hauber[b], M. Hilchenbach[e], L. Iess[j], P. Lamy[k], L.-M. Lara[l], P. Lognonné[m], J.J. Lopez-Moreno[l], H. Michaelis[b], J. Oberst[b], D. Resendes[n], J.-L. Reynaud[k], R. Rodrigo[l], S. Sasaki[o], K. Seiferlin[a], M. Wieczorek[m], J. Whitby[a]

[a]*Physikalisches Institut, Sidlerstr. 5, University of Bern, CH-3012 Bern, Switzerland*
[b]*Deutsches Zentrum für Luft- und Raumfahrt-Institut für Planetenforschung, Rutherfordstr. 2, D-12489 Berlin, Germany*
[c]*Bureau Gravimetrique International, Avenue Edouard Belin 18, F-31055 Toulouse, France*
[d]*Astronomy Institute, Sidlerstr. 5, University of Bern, CH-3012 Bern, Switzerland*
[e]*Max-Planck-Institut fuer Sonnensystemforschung, Max-Planck-Str. 2, 37189 Katlenburg-Lindau, Germany*
[f]*Royal Observatory of Belgium, 3 avenue Circulaire, B-1180 Brussels, Belgium*
[g]*Physikalische-Technische Bundesanstalt (PTB), Bundesallee 100, D-38116 Braunschweig, Germany*
[h]*Institute of Geophysics/Swiss Seismological Service, Swiss Federal Institute of Technology, (ETHZ), Honggerberg, CH-3093 Zurich, Switzerland*
[i]*Department of Astronomy, University of Maryland, College Park, MD 20742-2421, USA*
[j]*Dipartimento di Ingegneria Aerospaziale e Astronautica, Universita' degli Studi di Roma "La Sapienza", Via Eudossiana 18, I-00184 Rome, Italy*
[k]*Laboratoire d'Astrophysique de Marseille, Site Peiresc, Traverse du Siphon-Les Trois Lucs, 13376 Marseille Cedex 12, France*
[l]*Instituto de Astrofisica de Andalucia, C/ Camino Bajo de Huétor 24, 18008 Granada, Spain*
[m]*Département de Géophysique Spatiale et Planétaire/UMR7096-CNRS, Institut de Physique du Globe de Paris, 4 Avenue de Neptune, F-94100 Saint Maur des Fossés Cedex, France*
[n]*Instituto Superior Técnico, Universidade Técnica de Lisboa, Av. Rovisco Pais, 1049-001 Lisboa, Portugal*
[o]*Planetary Sciences Group, Geological Institute, University of Tokyo, Hongo, Tokyo 113-0033, Japan*

Received 26 July 2006; received in revised form 21 February 2007; accepted 2 March 2007
Available online 23 March 2007

Abstract

The BepiColombo Laser Altimeter (BELA) has been selected for flight on board the European Space Agency's BepiColombo Mercury Planetary Orbiter (MPO). The experiment is intended to be Europe's first planetary laser altimeter system. Although the proposed system has similarities to the Mercury Laser Altimeter (MLA) currently flying on board NASA's MESSENGER mission to Mercury, the specific orbit and construction of the MPO force the use of novel concepts for BELA. Furthermore, the base-lined range-finding approach is novel. In this paper, we describe the BELA system and show preliminary results from some prototype testing.

Keywords: Mercury; BepiColombo; Laser altimetry; Instrument design

1. Laser altimetry

Laser altimetry is a powerful remote sensing technique although the measurement concept is simple (Hofton et al., 2000). The time-of-flight of a pulse of light from a laser to a reflecting surface and back is measured (Fig. 1). The range from the laser to the illuminated spot on the surface is related to the laser pulse time-of-flight by

$$z = \frac{c\Delta T}{2}, \tag{1}$$

where $c = 299{,}792{,}458\,\mathrm{m/s}$ (Cohen and Taylor, 1997). Hence, a 1 ns delay is $\approx 15\,\mathrm{cm}$ range. This travel time,

*Corresponding author. Tel.: +41 316 314406; fax: +41 316 314405.
E-mail address: nicolas.thomas@space.unibe.ch (N. Thomas).

0032-0633/$ - see front matter © 2007 Elsevier Ltd. All rights reserved.
doi:10.1016/j.pss.2007.03.003

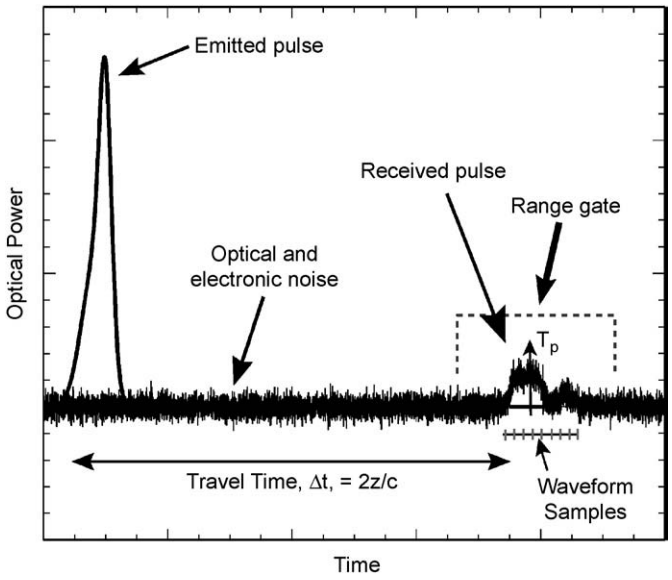

Fig. 1. Schematic of the time of flight measurement of a laser altimeter (after Bufton, 1989).

combined with ancillary information such as laser location and pointing at the time of each laser shot, enables the laser footprint to be geolocated in a global reference frame.

Laser altimetry can provide measurements of the structure and albedo of the target surface in addition to the straightforward range measurement. If $p(t)$ is the temporal dependence of the received number of photons in the return pulse, the three main parameters which can be extracted can be described as (Gardner, 1992)

$$N = \int_0^\infty p(t)\,\mathrm{d}t, \tag{2}$$

where N is the number of photons in the return pulse (a quantity related to the surface albedo)

$$T_\mathrm{p} = \frac{1}{N}\int_0^\infty tp(t)\,\mathrm{d}t, \tag{3}$$

where T_p is the pulse centroid time (a quantity related to the surface range) and

$$\sigma_\mathrm{p}^2 = \frac{1}{N}\int_0^\infty (t - T_\mathrm{p})^2\,\mathrm{d}t, \tag{4}$$

where Φ_p, is the RMS pulse width (a quantity related to the surface roughness and slope).

These quantities can be related to the properties of the surface by calibrations. For example, effective use of the number of returned photons requires at least a relative calibration of laser backscatter from different surfaces and a normalization by laser transmitter energy (Bufton, 1989).

After interaction of the laser footprint with a rough or sloping surface, the backscattered pulse may contain several nanoseconds or more of pulse spreading or distortion. The pulse width, therefore, gives basic information. Given that the transmitted laser pulse width is typically very short (1–10 ns or 0.15–1.5 m in altitude), this might be improved by application of GHz bandwidth digitization to the return laser pulse shape to provide information on the elevations and distributions of distinct reflecting surfaces within the laser footprint.

Early laser altimeter systems were flown onboard the Apollo 15, 16, and 17 missions. More recently, laser altimeters flown in space include the Shuttle Laser Altimeter (SLA), the Clementine laser altimeter, the NEAR Laser Ranging Investigation (NLRI) and the Mars Orbiter Laser Altimeter (MOLA). These missions demonstrated that metre-level topography of the Earth and other planets is routinely obtainable using this technique. Recent advances in ranging and processing techniques and the digital recording of the return laser pulse shape in airborne systems such as the laser vegetation imaging sensor (LVIS) show that decimetre-level of accuracy is now obtainable from medium-large footprint systems. All of these systems have used the "classical" (direct detection) approach to laser altimetry, which uses a high power laser (typically 20–50 mJ) at a low frequency (typically 1–10 Hz). For direct detection laser altimeters, typical return energies should result in values of 10^2–10^4 photons per pulse (Gardner, 1992; Zuber et al., 1992).

In this paper, we describe a design concept for a laser altimeter for the BepiColombo mission to Mercury. In the next section, we describe the aims, objectives, and mission specific issues, which the design concept must address. In Section 4, we describe the experiment and in Section 5 we discuss the expected performance based on numerical simulation. In Section 6, we discuss results of initial tests on key aspects of the proposed system.

2. Aims, objectives, and assumptions

2.1. Aims and objectives of the experiment

The BepiColombo Laser Altimeter (BELA) is a joint Swiss–German project with smaller involvements from Spain and France. The scientific objectives of the experiment are to measure

- the figure parameters of Mercury to establish accurate reference surfaces,
- the topographic variations relative to the reference figures and a geodetic network based on accurately measured positions of prominent topographic features,
- the tidal deformations of the surface,
- the surface roughness, local slopes and albedo variations, also in permanently shaded craters near the poles.

BELA will form an integral part of a larger geodesy and geophysics package, incorporating radio science and stereo imaging. Although stand-alone instruments in their own right, only the synergy between these will allow full scientific return. The synergy will cover the problems of planetary figure and gravity field determination, interior structure exploration, surface morphology and geology,

and extend into the measurement of tidal deformations. The offset between the centre of mass and the centre of figure will also be derived. The reference surfaces and the geodetic network will provide the coordinate system for any detailed geological, physical, and chemical exploration of the surface. The topography is needed to develop digital terrain models, which will allow quantitative explorations of the geology, tectonics, and age of the surface. The topography is further needed for a reduction of the gravity field data because topographical contributions to gravity must first be removed before using gravity anomalies for the investigation of sub-surface structures. The use of topography together with gravity data will constrain, by an admittance analysis between the two and with the help of a flexure model for the lithosphere, lithosphere and crust properties. Examples here would include the lithosphere elastic thickness (essential for the reconstruction of the thermal history of Mercury) and the crustal density (essential for the construction of a Hermean internal model). In addition to the moments of inertia, which will be provided by the radio science experiment, the tidal deformations measured by BELA and the radio science instrument will place further constraints of global models of the interior structure. BELA will contribute by providing the deformation of the surface while the radio science package will measure the mass relocations. Under favourable conditions, it will even be possible to constrain the rheology of the interior of the planet by measuring the time lag between the motion of the tidal bulge and the disturbing potential.

2.2. Mission assumptions

The design of the experiment assumes a mission design following the Announcement of Opportunity for BepiColombo issued by ESA. We note in particular the 400×1500 km polar orbit, the nadir-pointing panel through which the instrument observes the planet at all times, the 6 year cruise and 1 (Earth) year nominal mission duration. We have assumed that on one orbit, only one hemisphere needs to be mapped to have complete coverage of the surface of the planet over time. We further assume that the orbit will precess from a periapsis of 20° S latitude to 20° N latitude during the mission. Hence, to guarantee coverage of one hemisphere (pole-to-pole) we must acquire data up to 1055 km altitude.

The orbit design has several important implications. The orbital period is short (2.32 h) and comparable to the time constants for thermal equilibration of various hardware elements. Being permanently nadir-pointed implies that the Sun can illuminate any apertures up to an angle of 38° from the nadir direction immediately before or immediately after eclipse. Finally, the orbit also implies that the spacecraft can spend a significant amount of time over the dayside hemisphere at relatively low altitude and thereby receiving a large thermal IR flux. These elements make the thermal design of the laser altimeter considerably more challenging than any other system flown on space missions so far.

3. Experiment parameters

Through a signal to noise analysis, it has been shown that the Nd:YAG line at 1064 nm provides the optimum efficiency. Although detectors have a higher quantum efficiency at 532 nm, the lower albedo of the planet and the lower efficiency of the frequency-doubled laser make the 1064 nm line the better choice. In Table 1, we show how further experiment parameters must be derived. We discuss each element in turn.

3.1. Detection of return pulse

3.1.1. Link equation

The link budget scales the laser pulse energy and the receiver aperture area. The return pulse energy at nadir can be computed using the link equation:

$$E_r = E_t T_r \frac{S}{z^2} \frac{A_N}{\pi}, \tag{5}$$

where E_r is the received pulse energy, E_t is the emitted pulse energy, T_r is the receiver optics transmission, S is the collecting area of the telescope, A_N is the target surface reflectivity and z is the altitude of the spacecraft above the surface (Zuber et al., 1992; Abshire et al., 2000).

The quantity A_N/π is sometimes known as the target backscattering (coefficient) and has units of [sr^{-1}] (Bufton, 1989). This quantity has been the subject of considerable investigation. In particular, it must be estimated for zero phase angle (backscattering) geometry. The magnitude of the opposition effect on Mercury is unknown. Should this be similar to that of the Moon then one might expect an extremely strong return pulse. Hence for scaling our system we have had to select a wide range for Mercury and have used 0.10 to 0.40 for A_N at 1064 nm with a nominal value of 0.26 (Robinson et al., 1997).

Table 1
The design of the BELA system is driven by requirements in a rather specific order

Science requirement	System property driven
Detection of return pulse	Laser energy—receiver aperture area product (E_t A_r) Receiver electronics noise floor
Vertical (height) resolution	Laser pulse width and receiver electronics timing precision
Footprint size	Laser divergence angle and s/c altitude
Horizontal resolution along track	Repetition frequency
Elimination of solar background	Receiver field of view and filter bandwidth
Beam within R_x FOV	System alignment, receiver field of view

This table attempts to illustrate this. There are weaker interconnections, which are not noted here.

T_r is determined by the reflectivities of the telescope primary and secondary mirrors, the transmission of any refocussing optics, and the transmission of a narrow-band interference filter which is used to isolate the return pulse from other light sources such as straylight and reflected sunlight from the planetary surface. Accurate values for these quantities have been obtained by analysis and procurement. We currently assume that 63% overall transmission can be achieved.

The figure of merit used to quantify the performance of a configuration is the probability of false alarm (PFA). Although there are several possible ways to define this quantity, we choose it here to represent the probability that the system will fail to detect the return pulse. It should be clear from Eq. (5) that, assuming the instrument has the highest transmission, the product of E_t and A_r defines the received pulse energy, which in turn is linked to the PFA. Improvements in the PFA can be made by using previously obtained good returns to predict the time of future returns (range tracking). It should be clear that if a large number of false detections are generated, not merely will the data product be affected but the instrument will not be able to track reliably and hence will not be able to maintain tracking—leading to further false detections.

Two other critical values are required for PFA calculations. Firstly, the detector will be an avalanche photodiode (APD). The signal from the APD must be amplified. It has been recognized that the noise floor of the APD-amplifier combination has a significant effect on the PFA when close to the detection threshold of the system. Secondly, if the return pulse is spread, the noise becomes more dominant and a peak in the APD signal is less easily identified. A spread of the return pulse can be produced by surface slopes, surface roughness, and off-nadir pointing.

Hence, in our signal-to-noise calculations there are 5 major variables (Table 2). Of lesser importance are the laser divergence angle, the solar background, and the outgoing laser pulse width. All these factors have been included in detailed models of the system. The nominal values for the major inputs and the resultant E_tA_r are given in Table 2. Values for the E_tA_r product of $1.57 \times 10^{-3}\,J\,m^{-2}$ appear to offer acceptable solutions for justifiable values of the other parameters leading to a 20 cm diameter telescope if a 50 mJ pulse energy were to be considered optimal. From our thermal and mass analyses, a 25 cm diameter telescope forms an upper limit leading to a stringent requirement of at least 31 mJ for the laser pulse energy.

Table 2
Major variables affecting the probability of false alarm

Variable	Nominal value (range)
Energy-aperture area product, E_tA_r	$\geqslant 1.571 \times 10^{-3}\,J\,m^{-2}$
Amplifier noise	$\leqslant 1.7\,pA\,Hz^{-1/2}$
Surface slope (S)	3° (0°–18°)
Normal Albedo (A_N)	0.26 (0.10–0.40)
Altitude (z)	900 km (400–1055 km)

3.2. Range resolution and height measurement accuracy

3.2.1. Pointing and alignment

The range resolution of the altimetry measurement is determined primarily by laser pulse width and the timing precision of the altimeter electronics. With typical pulse durations and nano-second resolution timing electronics, metre or even sub-metre range resolution is achievable (Bufton, 1989). If the signal can be detected at all, then making a time-of-flight measurement to the metre level is not an issue. We note that the MESSENGER Laser Altimeter (MLA) (Solomon et al., 2001) will make measurements to an accuracy of 12 cm (Krebs et al., 2005).

However, a very essential ingredient in measurement of surface topography by laser altimetry is an independent knowledge of altimeter platform pointing angle and motion. Variations in laser pointing angle can map directly into biases and platform vertical motion can be confused with topographic variability (Fig. 2). In space-based laser altimetry, pointing angle effects are important because of the several hundred kilometres lever arm of the spacecraft orbit that maps angle into a bias in the derived altitude (Bufton, 1989). Hence, high-resolution laser altimetry requires some pointing control to maintain alignment near nadir and requires extremely accurate knowledge of altimeter attitude to compute angular offset from nadir and preserve height measurement accuracy (Fig. 2). The interaction of a finite beamwidth, θ_T at an angular offset, ϕ, from nadir and a surface slope can also produce

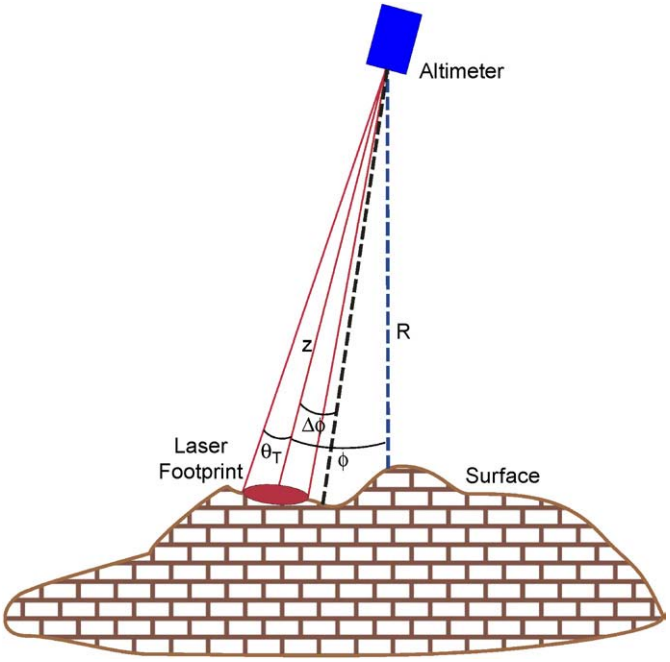

Fig. 2. Concept of laser altimetry with off-nadir pointing angle ϕ and surface slope, S. The outgoing laser pulse has a divergence, θ_T. The off-nadir pointing angle may only be known to an accuracy of $\Delta\phi$. The distance to the surface from the altimeter is specified as z while h is the height of the surface above a reference surface (and therefore describing the local topography).

significant spread beyond the nominal laser pulse width. Attitude must be measured by the spacecraft to $\leqslant 50\,\mu$rad for each laser pulse if, for example, metre-scale altitude measurement precision is to be maintained.

The height of the surface at the laser footprint, h, can be written as

$$h = \sqrt{R_{s/c}^2 + z^2 - 2R_{s/c}z\cos\phi} - R_{ref}, \quad (6)$$

(Abshire et al., 2000) where $R_{s/c}$ is the height of the spacecraft orbit above the centre of mass, ϕ is the pointing angle with respect to nadir and R_{ref} is the height of a reference surface for the planet (which is often taken to be the geoid).

Brenner et al. (2000), based on the papers of Gardner (1982, 1992), give equations for the mean pulse delay. The expected mean pulse delay is composed of the propagation delay along the centre of the laser beam, the additional delay resulting from phase front curvature of the diverging laser beam, and the biases caused by off-nadir pointing and pointing jitter. It is given by

$$z(T_p) = \frac{2z(1+\tan^2\theta_T)}{c\cos\phi}[1+(1+2\tan^2(\phi+S_x)]\frac{\sigma(\Delta\phi_x)^2}{2} + \cos^2\phi\left(1+\frac{2\tan^2 S_y\cos^2 S_x}{\cos^2(\phi+S_x)}\right)\frac{\sigma(\Delta\phi_y)^2}{2}, \quad (7)$$

where S_x and S_y are the surface slopes in the xz and yz planes, respectively, $\Delta\phi_{x,y}$ is the pointing error parallel and perpendicular to the pointing direction, and ϕ is the off-nadir pointing angle. θ_T is the $1/e$ half-width of the laser beam divergence and is related to the FWHM by the equation:

$$\theta_{FWHM} = 2\theta_T\sqrt{-2\ln\frac{1}{2}}. \quad (8)$$

Gardner (1992) has provided simplified formulae, which allow quick estimates of height measurement errors assuming the spacecraft position is known perfectly. The dominant terms come from the spacecraft, not from the instrument. It should be noted that the final accuracy assessment requires information about uncertainties in the spacecraft position.

3.2.1.1. Laser pulse duration. Keeping the laser pulse duration small reduces the spread of the return pulse and, therefore, enhances PFA and centroiding. Pulse durations of 5–8 ns are usual. Both MLA and MOLA achieved this for comparable pulse powers. Investigations with a verification model of the proposed laser for BELA give pulse durations of around 3 ns.

3.2.1.2. Rangefinder electronics. There are several approaches to the rangefinder electronics. Each have advantages and disadvantages. They breakdown into 3 groups (Table 3).

The problem of identifying the return pulse is one of detecting a known signal with unknown time of arrival (Anderson and Qatshan, 2001). A well-known approach is that of matched filtering (Kay, 1998) which can be solved using the generalized likelihood ratio test (GLRT).

MOLA used matched filters followed by leading edge detection in analogue. GLAS used matched filter detection followed by direct transmission of the entire waveform around the point identified by the matched filter. For BELA, the baseline is to use matched filters in digital (an field programmable gate array, FPGA) followed by improving the initial result in software.

It can be shown analytically (Gunderson et al., 2006) that detection will be maximized using a 10–20 MHz filter to smooth the signal prior to 80 MHz sampling and matched filter convolution. This corresponds to 1.87 m per sample or 3.74 m per resolution element for the coarse detection.

Extracting higher moments of the return pulse allows the study of surface structure within the footprint. There are two possible approaches. Either the digitized data (with consequent effect on data volume) can be downlinked or higher moments (skewness and kurtosis) can be extracted in software (with effect on the CPU load). Both approaches are possible within the current design.

3.3. Footprint size

The size of the footprint has an effect on the PFA—the larger the footprint, the wider the return pulse. Hence small laser divergence angles are preferred. However, very small

Table 3
Groups of rangefinder types that are possible for BELA

Type of rangefinder	Example	Advantages	Disadvantages
Analogue leading-edge detection	NLRI	Potentially extremely accurate (MLA at 12 cm)	Thresholding in combination with leading edge leads to range walk
Analogue leading-edge detection with subsequent digitization of waveform	GLAS	Timing extremely accurate followed by waveform downlink for Earth-based processing	Large data volume
Digital detection	BELA (baseline)	Peak exactly identified (no range walk). Detection in soft (or firm) ware.	Lower range accuracy because of speed of digitization. Digital waveform transmission possible if data volume allows

divergence angles require high magnification and large optics. The compromise has been set at 50 μrad full cone angle. This value drives the beam quality of the laser itself and the magnification of the beam expander (BEX).

3.3.1. Beam quality (M^2)

M^2 is a common measure for the beam quality of a laser beam. According to ISO standard 11146, it is defined as the beam parameter product (the beam radius measured at the beam waist and the beam divergence measured in the far field) divided by λ/π, the latter being the beam parameter product for a diffraction-limited Gaussian beam of the same wavelength. In other words, the beam divergence is given by

$$\gamma = M^2 \frac{\lambda}{\pi w_0}, \tag{9}$$

where w_0 is the beam radius (radius with $1/e^2$ intensity) at the beam waist. The beam parameter product is usually expressed in units of [mm mrad]. The minimum beam parameter product for a 1064 nm Nd:YAG beam is 0.339 mm mrad.

A beam quality requirement of $M^2 \leqslant 1.6$ has been set for the BELA laser. A verification model of the laser has been developed and has achieved this level of performance.

3.3.2. Beam expander

The BEX must match the divergence of the laser to the required footprint size. The present design gives a clear aperture diameter of 45 mm. Using Eq (9), we obtain a beam divergence (half-cone) of 24.1 μrad. The nominal divergence of the MOLA laser was $\gamma = 93$ μrad (Abshire et al., 2000). Based on this value, Neumann et al. (2001) predicted larger pulse widths over sloping terrain than were observed. Using inflight data and the Gardner (1992) model to estimate γ, the divergence was found to be 0.5 times nominal, owing to hot spots in the laser beam. The BELA laser system is seeking to minimize such hot spots, which could lead to more rapid degradation of the crystal.

3.4. Horizontal resolution

The horizontal resolution of the instrument along track is a compromise between topographic information (driving to high pulse repetition frequency) and power consumption (driving to lower frequency). There appears to be no clear-cut scientific advantage of (say) 12 over 10 Hz. Our approach is to baseline 10 Hz and to investigate in detail the system properties. This corresponds to 258 m between pulses at periapsis.

The spacecraft ground-track defines the cross-track spacing and is equal to 25.3 km at the equator for the current mission design. At periapsis, the spacecraft would be required to turn by 3.62° to view the previous ground-track. BELA has been designed to allow this manoeuvre.

3.5. Elimination of solar background

The solar flux reflected from the surface interferes with the pulse detection. The background photon rate can be computed from standard radiometric relationships (e.g. Cole, 1996). The use of an interference filter to minimize the reflected background is mandatory. The bandwidth must be traded against the transmission of the narrow-band filter (which affects the signal and hence the PFA) and the wavelength of the laser. The TEM_{00} mode of the Nd:YAG is at 1064.1 nm. However, there is another line at 1064.6 nm. The relative intensities for these two lines is not yet known. A $\Delta\lambda$ of 1 nm (FWHM), therefore, appears to be the best solution. A transmission of 80% for such a filter has been obtained in commercial developments.

4. Baseline design

The baseline system is shown schematically in Fig. 3. Laser altimeters are bistatic systems, with the transmitter separate from the receiver (Cheng et al., 2000). Bistatic designs allow the transmitter and the receiver to be addressed separately, thereby reducing complexities in transmit/receiver switching (which decreases signal power) and permitting parallel development of the transmitter with the receiver (Cole, 1996). This allows the BELA instrument to be developed in two countries in an effective manner with Germany taking responsibility for the transmitter and Switzerland leading the development of the receiver.

4.1. Transmitter

4.1.1. Laser sub-system

The baseline laser design is a longitudinally pumped passive Q-switch Cr-doped Nd:YAG laser operating at 1064 nm. Longitudinal pumping has an advantage over conventional side-pumped lasers in that the absorption path length can be longer making the laser less sensitive to temperature variations of the pump diodes.

There are three main elements (Fig. 4).

- The laser electronics unit (LEU) contains the capacitor bank and the power distribution system for the laser. It is mounted to the spacecraft experiment platform.
- The pump diode unit (PDU) contains the laser pump diodes and associated optics. The PDU is connected to the LEU through a short cable. It is mounted to the spacecraft experiment platform.
- The oscillator and amplifier box (OAB) contains the laser bench. It is mounted to the instrument baseplate (BP). It is connected to the PDU through a fibre-optic cable.

The baseline specification for the laser pulse energy is 50 mJ (BOL). The concept for the laser is shown in Fig. 5.

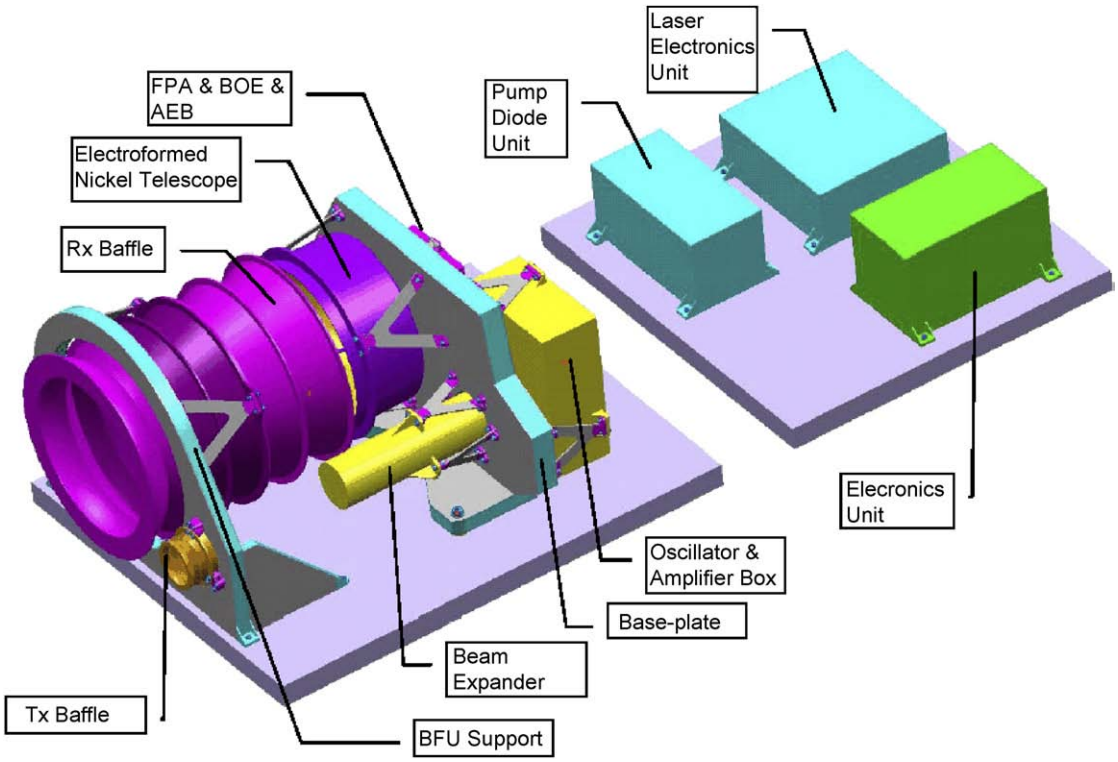

Fig. 3. BELA mechanical configuration showing the major elements of the system.

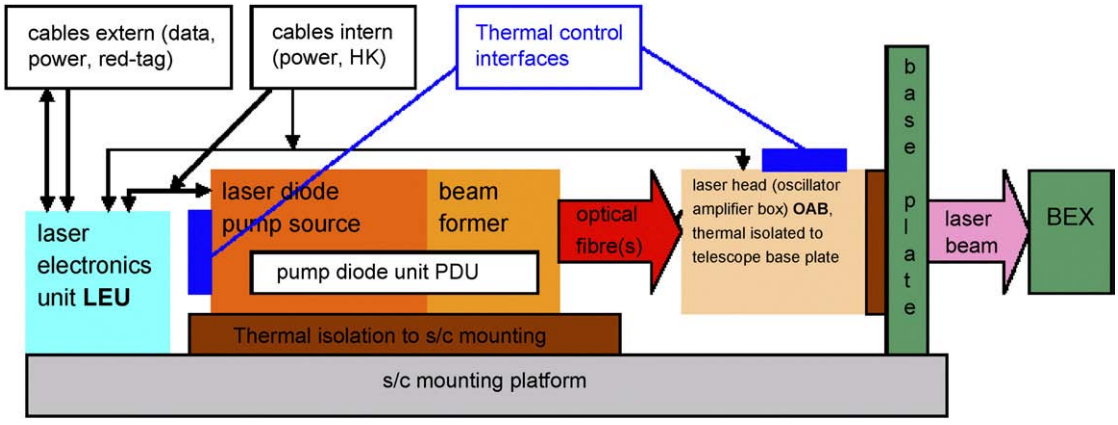

Fig. 4. Schematic diagram of the main components of the laser.

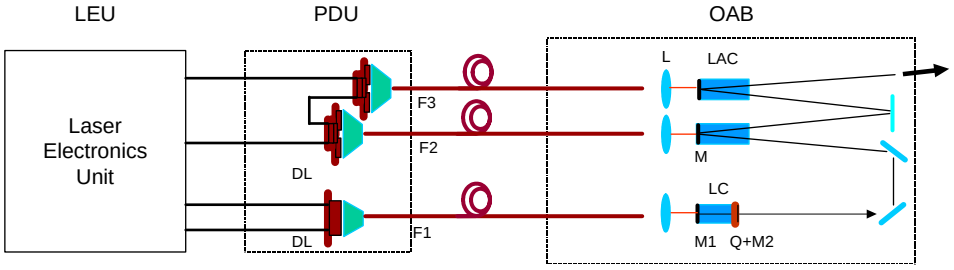

Fig. 5. Concept for the BELA laser (copyright: vH&S, LZH, EADS, DILAS). DL: Diode Laser Stack, MBI: Miniaturised Beam Integrator, F: Fibre, BS: Beam Splitter, CL: Collimator Lens, LC: Laser Crystal, M: Mirror, Q: Q-Switch Crystal. (*Source*: Industrial BELA Laser Consoritum).

4.1.2. Beam expander

The BEX takes the output from the OAB and produces a 50 μrad divergence beam based on the assumption of $M^2 \leqslant 1.6$.

The BEX consists of the following main components (Fig. 6):

- Tubular housing.
- Optical elements with mountings.
- Fibre interface to the start electronics.

The laser beam enters the BEX through an afocal BEX, which expands the beam by about a factor of 20. The beam is parallelized by a larger exit lens (–group). The optical distance between these two lenses is about 0.2 m. The divergence will be reduced by the same factor. An incoming beam with a radius of 1 mm and a divergence of 1 mrad will be expanded to an outgoing beam with the radius of 20 mm and a divergence of 50 μrad. Before the expanded beam exits the BEX, the optical alignment will be established using two wedge prisms. By rotating the two prisms, the boresight of the beam can be adjusted parallel to the telescope boresight. The laser has to be protected against straylight (or sunlight reflected from the surface of Mercury) provoking spontaneous emission and hence the front sapphire window of the BEX has been coated to block incoming radiation. This has been accounted for in the PFA calculations.

MLA experienced a problem that feedback from the BEX destabilized the laser oscillator. In this case, the laser team increased the angle of incidence on the BEX to 7.5 mrad and added a polarizer and 1/4 wave plate to the laser optical train to add optical isolation (Ramos-Izquierdo et al., 2005). It is intended to implement a similar approach.

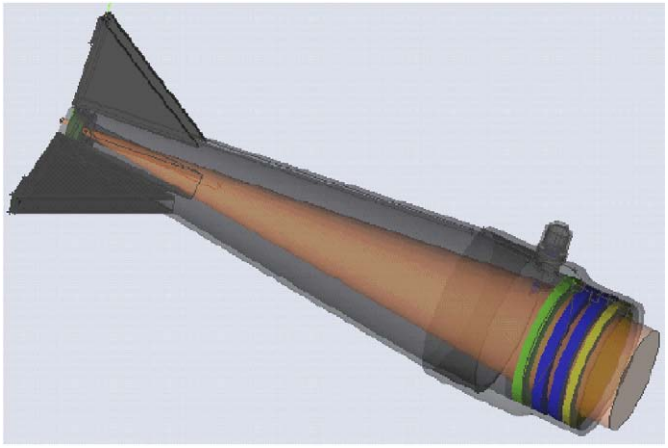

Fig. 6. Mechanical concept for the BEX. The beam (shown in light orange) enters from the left and passes through a concave lens (dark green). The second (green) lens is followed by two alignment prisms and a sapphire (coated) window.

4.1.3. Start pulse optical assembly

An additional optical assembly in the BEX, the fiber interface, picks off a small part of the laser light which is then taken via a fiber cable to the start electronics in the ELU, which, in turn, detects and measures the temporal beam profile (Fig. 7).

4.2. Receiver optical system

The receiver optical system consists of:

- Reflective baffle, reflecting sunlight and a major part of the planetary flux.
- $F/5$ telescope ($f = 1250$ mm, Ø250 mm), with focal point at the vertex of the primary mirror and realized as a pinhole, preventing the planetary flux reaching the back-end optics (BEO).
- BEO for purpose of spectral filtering and wave front correction.

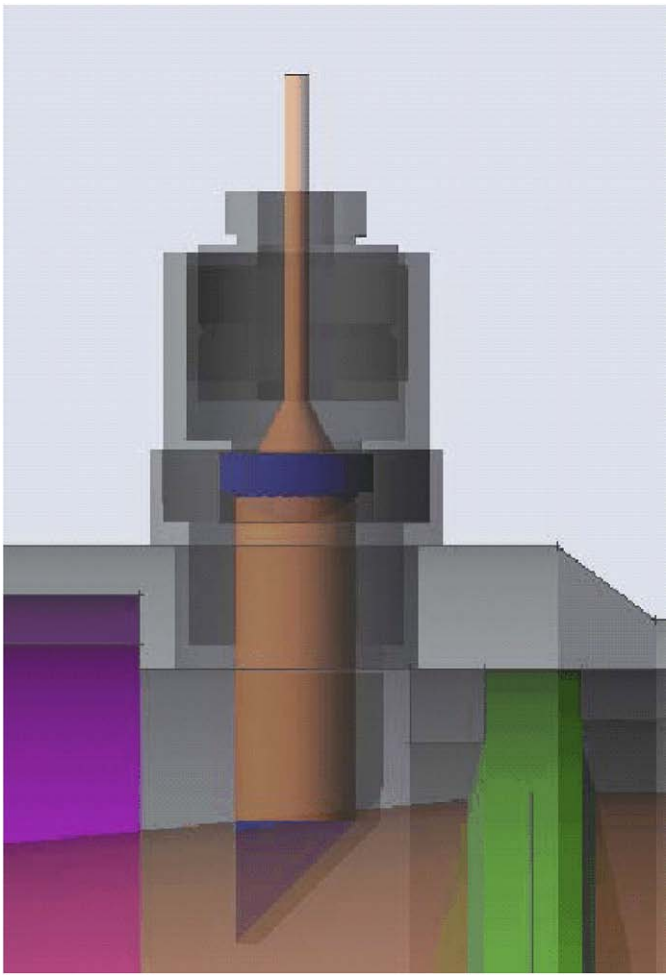

Fig. 7. Fibre-optic interface to the BEX pick-off light from the collimating lens and passes it to the ELU.

4.2.1. Telescope (ENT)

The telescope design is based on a system already developed and manufactured by Media Lario (Lecce, Italy). The lightweight telescope concept is based on nickel-electroforming technology, which has been developed to produce the mirrors for the XMM/Newton Space Telescope (Fig. 8). The replicated mirrors have a thickness of <1 mm down to 0.3 mm and thus outstanding low mass versus collecting area. The electroforming process guarantees a very homogenous coefficient of thermal expansion (CTE), which is of great advantage for an athermal configuration. The ENT has been tested and successfully passed electro-magnetic compatibility tests. Work is currently on going to determine its behaviour when exposed to a high thermal infrared load simulating the planetary IR flux. Alternative approaches to the telescope (including use of a beryllium which has superior mechanical properties) are also still under discussion.

4.2.2. Receiver baffle (BFL)

A baffle is required to eliminate off-axis sunlight between 38° and 90° from the boresight. It is one of the major differences in design requirements compared with the MLA and, to our knowledge, novel in its application to space.

Unlike most optical systems, the baffle must be reflective since blackened surfaces would lead to absorption, intolerably high temperatures, and high thermal input to the spacecraft. The concept of reflective baffles is not new (e.g. Kleinhans, 1976) and several publications have described possible systems (Stavroudis and Foo, 1994 and refs. therein).

The design solution (see also Seiferlin et al., in revision) consists of an alternating sequence of ellipses and hyperbolas (Fig. 9), which all have their origins in the centre of the entrance aperture and the two focal points at the edge of the entrance aperture.

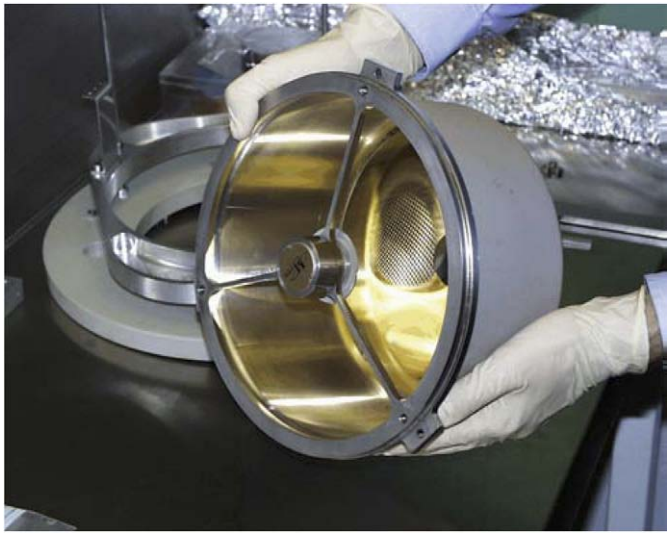

Fig. 8. Media Lario lightweight telescope considered as baseline for BELA.

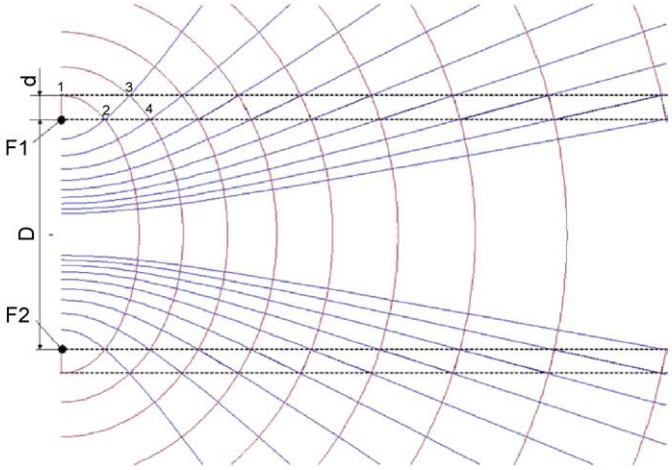

Fig. 9. Design concept for the specular baffle.

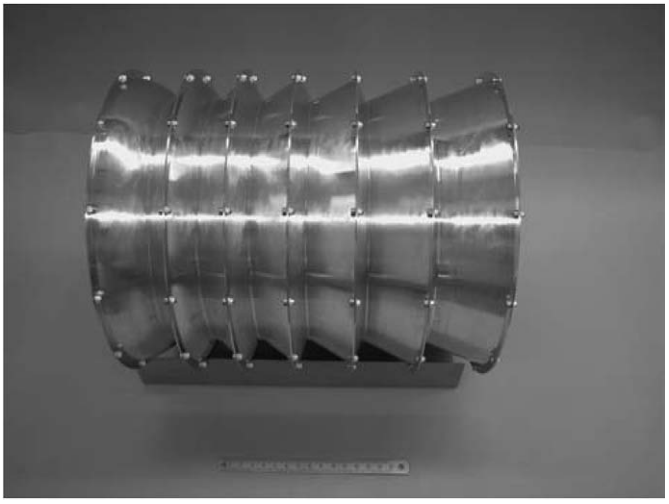

Fig. 10. Reflective baffle produced by UBE. The aluminium structure has a 20 cm inner diameter and weighs 716 g.

The optical design of this kind of baffle is completely determined by the specification of the clear aperture D, the outer diameter $D+2d$ and the maximum available length L. In practice, where D and L are a priori known, d is tuned, within the available envelope, such that the design arrives with a complete ellipse at the end. There are no more degrees of freedom.

To verify the mechanical concept, the interfacing between the vanes, and the overall mass, a bread-board system has been manufactured from aluminium (Fig. 10). Fig. 11 shows the spectral performance of a prototype coating and calculated values for the absorption under solar and Mercury illumination. The power absorbed averaged over one orbit is at most 9.5 W. The peak is around 27 W. This forms an upper limit because the spectral reflectance measurements only go out to $\lambda = 2.5\,\mu$m.

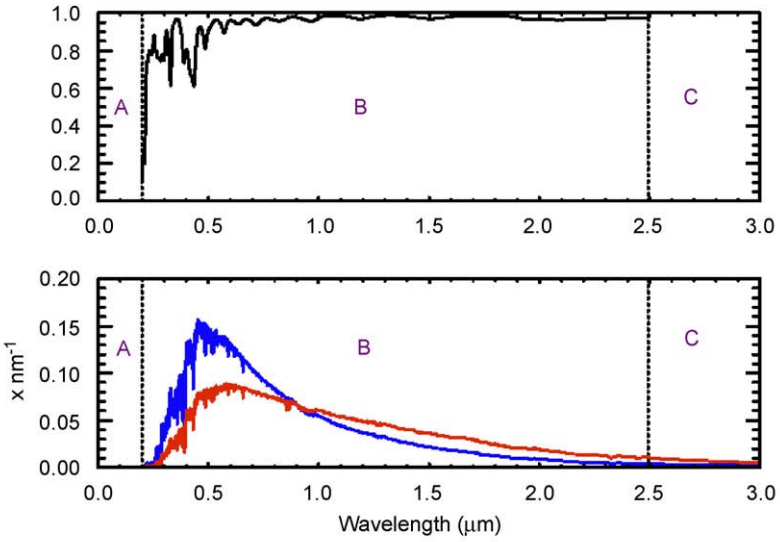

ABSORBED FRACTION OF INCIDENT SPECTRA						
	A	B	C	Range	Peak P (W)	Peak average power orbit^{-1} (W)
Solar	0%	6.7%	<3.1%	0.07-0.10	18-27	4.7-7.0
Mercury	0%	4.4%	<8.7%	0.04-0.13	2-6	0.8-2.5

Fig. 11. Top: reflectivity of a coating proposed by Thin Film Physics, Regensdorf for the UBE aluminium baffle. Middle: Solar and Mercury-reflected flux distributions. Bottom: computation of the absorbed incident power. (A–C) correspond to wavelength ranges over which the calculation has been performed. Note the peak power and the orbit-averaged power absorbed by the baffle.

4.2.3. Back-end optics

The ENT will be manufactured with only a small hole in the primary through which the beam will pass. This approach has two substantial advantages.

- The telescope forms an enclosure against the incoming reflected and thermal radiation from Mercury, thereby limiting heat transport into the spacecraft and only allowing a small amount of power (fractions of a Watt) to enter the back-end of the instrument.
- If the spacecraft goes into safe mode while in eclipse and emerges with the Sun directly along the nadir axis (and, therefore, along the telescope boresight) the load on the BEO, the interference filter, and the detector can be kept low (<1 W) thereby eliminating the need for a protection mechanism. We note that MOLA was tested against this eventuality (Ramos-Izquierdo et al., 1994).

The system requires a transfer optic to focus an image of the pinhole onto the focal plane. However, a further advantage is that the hole in the primary can be used to define the field of view and hence small changes in the optimum focal length of the receiver need have little influence on the BEO. A larger hole in the primary is assumed for manufacturing reasons and a pinhole mounted to the BP directly in front of the BEO. The design can be easily adapted for Schott BK7G18 (radiation resistant) glass. The transmission at 1064 nm is nearly 100%. The back-end triplet for MLA was also made from BK7G18 (Ramos-Izquierdo et al., 2005). An interference filter must be placed within the BEO to eliminate reflected solar background (see above). The central wavelength of the filter (1064 nm) will be sensitive to temperature (see e.g. Ramos-Izquierdo et al., 1994). A value of around $\Delta\lambda/\Delta T = 2 \times 10^{-5}$/K is expected.

4.3. Detector and analogue electronics

4.3.1. Detector, amplifier and cooling

Following a trade-off study, the Perkin-Elmer C30954E APD has been baselined (following MOLA). The quoted noise floor of the PE device is $2\,\mathrm{pA}/\sqrt{\mathrm{Hz}}$. PE manufacture a package (C30569-1060-R8B) consisting of a C30954E APD with a GaAs FET preamp in close proximity, which reaches $1.7\,\mathrm{pA}/\sqrt{\mathrm{Hz}}$ at a bandwidth of 200 MHz. By increasing the resistance, the bandwidth might be reduced to that required by BELA and hence further noise reductions ($1\,\mathrm{pA}/\sqrt{\mathrm{Hz}}$) may be possible. This is the subject of ongoing investigation. The APD, proximity electronics and a Peltier element will be mounted in a focal plane assembly (FPA). A high voltage (300 V) supply, needed for the APD, will be placed in close proximity to the FPA.

The surface reflectance properties and surface roughness of Mercury are at present poorly known, especially at 1064 nm and in opposition geometry. Therefore, a key problem is the question of how to handle a potentially extremely large dynamic range of the return pulse. The baseline solution is to use a variable gain amplifier with

logarithmic steps over a range of >1000. The instrument will be designed to perform gain setting switching autonomously.

4.4. Rangefinder (signal processing)

4.4.1. Digitization and coarse detection

It is foreseen that after smoothing with a 10–15 MHz bandpass filter, the signal will be sampled by a 12 bit ADC. Digitization results in

- low complexity of the system,
- relatively low power consumption and
- reconfigurability.

The frequency of the sampling is currently under discussion. The current baseline is to use 80 MHz samples. After digitization, the signal passes to an FPGA, which performs a coarse detection of the return pulse using the matched filter concept, following MOLA. Unlike MOLA, however, the choice of which filter matches best can be made by signal to noise calculations onboard and is programmable. This is a novel part of the instrument.

The rangefinder electronics receives the time of the start pulse from the digital processing unit (DPU) and calculates the time of flight based on its knowledge of the receive time. This forms the basic measurement that BELA can make and is very robust at low SNR. Depending upon the best-matched filter chosen, an estimate of the pulse width is also obtained.

4.4.2. Digital downlink and fine detection

Once the coarse detection has been made, the baseline offers three options.

- Downlink of coarse detection results only.
- Downlink of coarse detection results plus the digitized signal about the detected return.
- Application of a fine detection routine (sub-sample fitting of the return pulse) on the instrument's computer with downlink of the results from this calculation.

  For the fine detection, range and pulse spread estimation is done by a fitting approach rather than simple thresholding (as for example MOLA). This results in
- simplified calibration and
- unbiased measurements (no range walk).

The present software system is somewhat inferior in range accuracy to MLA but still within the BepiColombo science requirements. Return of skewness and kurtosis parameters to give pulse shape information must be traded against processing power requirements and can only be assessed after test coding.

4.4.3. High speed digitization

An approach to high-speed sampling (1 Gsample/s) of the return pulse was also studied and implemented as a bread-board. A similar approach was used on GLAS. However, the resource requirements for the system in terms of mass, power, data volume and additional complexity (although modest) were considered to be too high to implement for the BepiColombo mission.

4.4.4. Acquisition and tracking

There are two algorithmically distinct but closely related procedures that are required.

Range window tracking deals with the problem of finding the range window within which the return signal is expected to arrive (the global picture). Apart from the sampled data, there will be additional (a priori) information available that should be taken into account for best acquisition efficiency, e.g. orbit data provided by the spacecraft. The width of the range window (or range gate) must be very much smaller than the full range of altitudes for BepiColombo. This effectively sizes a FIFO, which reads out the APD and is restricted to values of less than about 30 km in equivalent altitude range.

Range tracking deals with the problem of pulse detection within the measured range window. Once the pulse is detected, the objective is to track within the range window and, by taking account of a priori information (e.g. the orbit), minimize the PFA. Obviously, this would include moving the range window when required.

For both procedures, a Bayesian approach (a common concept in laser altimetry—see e.g. Luthcke et al., 2000) of maximizing the probability of detection is taken. Range tracking with this approach has already been implemented in trial software. The basic concept is that inputs to the software can be assigned probability distributions, which are used to optimize the search for the signal or to maintain it tracking.

The software must keep track of the previous pulses to form of a picture of the terrain it is crossing. Numerical experiments suggest that knowledge of 5–6 of the previous pulses must be retained to maintain a stable tracking. This description also shows how the spacecraft orbit data can be used. The experiment knows where the spacecraft thinks it is with respect to the centre of mass. Hence, as we know roughly the radius of Mercury, we can set up a probability of a detected signal being a true return or not and begin to narrow the range gate on that basis to reduce further the PFA. This type of approach is being used in many applications (e.g. Sheppard and Kaufmann, 2005).

4.4.5. Start pulse detection

The laser uses a passive Q-switch and, therefore, the exact time of emission is not known a priori. This problem is resolved by using start pulse detection electronics. A fibre takes scattered light from the BEX to the electronics box where a board containing a PIN diode is located. The electronics generates a signal when the outgoing pulse is emitted which is sent to the DPU and the rangefinder electronics. The rangefinder electronics performs the time-of-flight measurement.

The baseline is to digitize the outgoing pulse with 8 bit resolution at 500 MHz (2 ns). This has the important advantage of allowing us to monitor changes in the emitted pulse in flight. With the digitizer, we can determine the amplitude and shape of the pulse and thereby monitor deterioration of the laser in flight and correct for this behaviour. To save power, this will only be performed upon request from the DPU. Should the first versions of the laser prove to give extremely narrow pulses (<5 ns FWHM) then descoping of this capability may occur.

The optical receiver is an InGaAs pin photodiode with a fibre and a transimpedence amplifier. The TIA has been selected for high bandwidth (2 GHz). The remaining circuitry contains differential amplifiers, a delay line, a clock, trigger and clock distribution, ADC, bias control, and an FPGA.

4.4.6. Oscillators and clocks

In order to make a time-of-flight measurement, the system requires a clock. Within BELA, the system must resolve time differences of around 2 ns over a flight time of about 6 ms—an accuracy requirement of about 1 part in 3×10^6. We have chosen 1 part in 10^7 as our target. BELA will internally use a high-frequency low-jitter clock signal. The key issue with this oscillator is knowledge of the oscillator frequency over long periods.

The alternative to high stability and high mass systems, which must maintain their frequency over 6+ years and in a difficult thermal environment, is to calibrate the oscillator frequency. This can be done in one of two ways. Both GLAS and NLRI used a long (100 s m) fibre-optic cable as a delay line to measure a known distance and thereby calibrate the system. This approach requires mass and a large investment in qualification of the fibre-optic (see for example, Ott et al., 2003).

BepiColombo and BELA intend to follow an approach similar to that on MOLA. This requires that the spacecraft provides BELA with a reference time signal against which the internal oscillator can count. To avoid high long-term stability requirements on the spacecraft oscillator, the spacecraft oscillator should itself be calibrated against the radio-transmitter oscillator (it could in principle be the same oscillator), which in turn could be verified by the ground station.

4.5. Electronics unit

4.5.1. Interfaces

Careful attention has been paid to interfaces in the electronics as there are several important issues to be resolved. The electronics are enclosed in a box sketched in Fig. 12.

The ELU (sometimes referred to synonymously as E-box) interfaces to the spacecraft via the SpaceWire IEEE 1355.2 standard interface. The ELU contains a DPU, which performs this function.

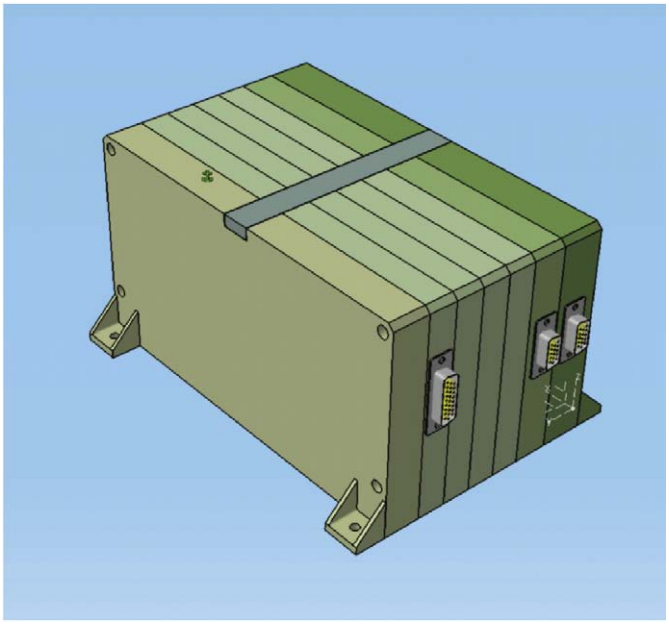

Fig. 12. CAD/CAM model of the electronics unit.

The DPU interfaces to

- the rangefinder (receiver) electronics via a synchronous serial data interface,
- the LEU to acquire HK and to initiate or shut down the laser sub-system,
- the power converter module (PCM) to collect HK,
- the start pulse electronics.

4.5.2. Digital processing unit

4.5.2.1. Functions. The DPU acts as an instrument processing- and control front-end. It is located together with the power converter, the receiver electronics, and the start electronics in the ELU. The DPU will perform the following tasks:

- Reception of telecommands and their decoding.
- Reception of the START and STOP signals.
- Reception and processing of the digitized receiver signal.
- Control of the sensor operation.
- Data compression (if any) and telemetry formatting and transmission.
- HK data acquisition.
- Instrument health check.
- Software upload support.

4.5.2.2. Hardware. The BELA–DPU consists of the following sub-systems (Fig. 13):

- FPGA with the LEON-FT processor core and other dedicated digital control logic.
- PROM (64 Kb) and EEPROM Memory (512 Kbytes) for boot- and program storage.

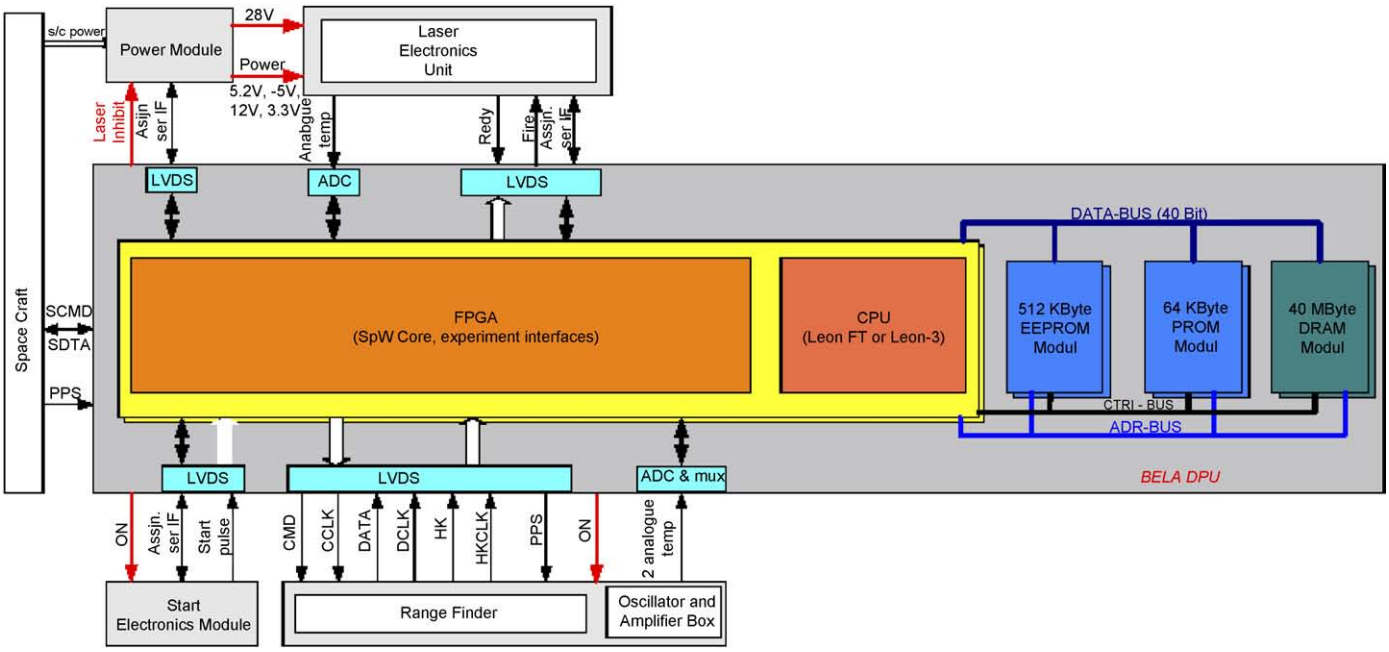

Fig. 13. Block diagram of DPU functionality.

- 40 Mb SDRAM-memory for data storage (32 Mb net due to EDAC).
- Spacewire data- and command interface.
- HK interface incl. MUX and ADC.
- Instrument control interfaces.
- Asynchronous serial interfaces to power supply and laser electronics.

4.5.3. Power converter module

The PCM consists of a dedicated power supply unit which distributes a specific number of voltages to the BELA instrument subsystems. It is located inside the ELU-Box.). The PCM converts power from the spacecraft to the voltages needed by the other subsystems inside the E-box, the laser unit and the analogue electronic box (AEB), which is mounted to the BP (close to or incorporating the detector). Additionally, it provides electrical isolation between primary and secondary sides of the unit. Design drivers for the proposed architecture are the following basic requirements:

- The PCM should be redundant.
- After primary power ON (nominal or redundant branch) the BELA instrument should be switched on without any extra Power Relay commands from S/C side.
- For diagnostics the functional components of BELA should be switchable (power on/off) separately (Identified components are: DPU + S/C IF, range finder including proximity electronics, start electronics, laser electronics).
- Implementation of a laser inhibit switch (also hardwired and extern removable) to enable laser diode pumping.

The PCM shall have two primary power inputs, main and redundant, from the spacecraft power subsystem. The PCM provides the filtering, isolation and over-current detection on the primary side to the spacecraft interface.

4.6. Resources

The mass of the experiment is currently estimated at 10.8 kg with a margin of 1.3 kg. Under the assumption of a repetition rate of 10 Hz, the secondary power requirement is 32.4 W. Assuming a 75% DC/DC converter efficiency we obtain 43.2 W primary power. Estimates for the required data rate depend upon the mode used. For nominal tracking mode with fine detection and including regular housekeeping, the data generation rate is estimated at 1130 bit/s. For a total of 1.5×10^7 s of operation (1 Earth year operating with a 50% duty cycle), we expect a total data volume of 2.2 Gb.

5. Expected performance

The major variables, which are not under our control (see Table 2) are:

- the normal albedo (A_N) of the surface,
- the altitude (z),
- and the surface slope (S, which contributes to σ_p).

If these three quantities are set to extreme conditions, there is a danger of over-sizing the system. To prevent this, a nominal measurement condition has been defined (Table 4) which encompasses most of the expected cases. A limited measurement condition, taking into account

Table 4
Definitions of nominal and limited measurement conditions

	Nominal measurement conditions	Limited measurement conditions
A_N	$\geqslant 0.18$	$\geqslant 0.10$
S	$\leqslant 3^\circ$	$\leqslant 23^\circ$
Z	$\leqslant 900$ km	$\leqslant 1055$ km
PFA	$<10\%$	$<50\%$

possible extremes, has also been defined. A further design criterion is that if two conditions are only within the "limited" range but one is within the "nominal" range, then the PFA shall be $<20\%$.

Two independent models to simulate system noise characteristics have been produced which allow determination of probabilities of false alarm over a variety of conditions. An example plot is given in Fig. 14 and shows that the PFA for most realistic test cases begins to rise as the altimeter goes above 1000 km. This suggests that the proposed system is accurately designed for the mission scenario. Note that this plot also shows the effect of varying the field of view of the telescope (which affects the amount of background reflected light from Mercury and thereby affects signal to noise).

Remaining uncertainties in the PFA result from

- knowledge of the exact transmission of the BEX (resulting from the protective coatings),
- the precise value of the noise floor of the APD/amplifier,
- the exact thermal control of the APD.

Allowances have been made for these values, which should result in lower limits for the performance in our simulations.

On the instrument side, there remain small uncertainties on the ranging accuracy because the approach to the oscillator is still unclear on the spacecraft side. Once an adequate interface has been negotiated, we do not expect this to be a driver of the range accuracy.

6. Test and mercury simulation

6.1. Laser verification

A verification model of the longitudinally pumped laser has been produced by an industrial consortium led by von Hoerner and Sulger GmBH, the Laser Zentrum Hannover, DILAS and EADS under the supervision of the Max-Planck-Institut fuer Sonnensystemforschung. The system has achieved the performance shown in Table 5, which meets the requirements set for the laser sub-system. The present system is not flight representative, however, a prototype is now being planned for completion in mid-2006.

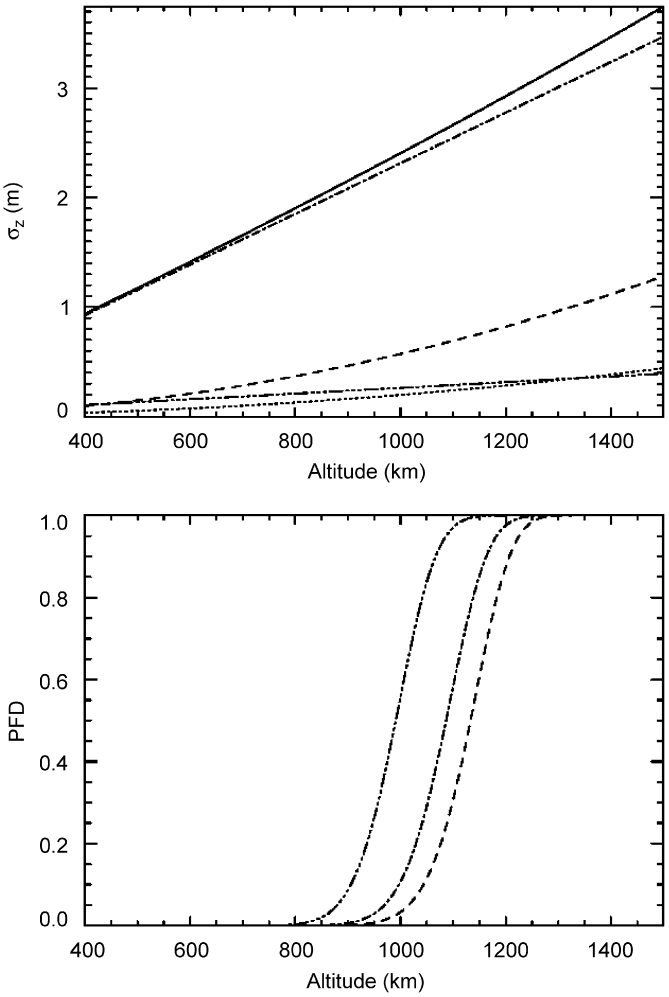

Fig. 14. Top: the range uncertainty according to the expressions of Gardner (1992). The plotted components represent uncertainties due to surface roughness (dotted), nadir/slope angle (dashed), spacecraft pointing uncertainty (dash-dot) and system errors (dash-dot-dot-dot). Total uncertainty is given by the solid line. Bottom: the probability of false detection versus S/C altitude for three different matched filters of 15 (dash-dot-dot-dot), 30 (dash-dot), and 60 ns (dash). The model used is described extensively in Gunderson et al. (2006) and has used the parameters given in the text.

Table 5
Pulse properties achieved by the verification model (VM) of the laser

Quantity	Value obtained
Wavelength	1064 nm
Pulse energy	52 mJ
Pulse frequency	10 Hz
Pulse duration	$<$ 3 ns
M^2	<1.5
Optical efficiency	23%

6.2. Mercury simulation

A major difference between MLA and BELA is in the requirements for thermal control. Unlike MLA, there is no sunshield to protect the instrument from direct sunlight

entering the aperture. In nominal operation, sunlight can reach 38° from the boresight just before the spacecraft goes into eclipse behind the planet. Furthermore, the Sun may be aligned with the boresight for as long as 3 min if the spacecraft exits eclipse having previously gone into safe mode. The baffle of BELA is designed to treat the nominal case

A Mercury environment simulator has been produced to simulate both the incoming solar flux and the Mercury thermal IR flux inside a thermal-vacuum chamber. The solar flux simulator uses a Xenon lamp to simulate the Sun. The beam is made approximately parallel using a parabolic mirror of 25 cm diameter. The beam passes through a Suprasil window into the vacuum chamber where it strikes a plane mirror. The angle of the plane mirror can be adjusted to simulate solar incidence angles of 38°–90°. The beam is reflected onto the baffle, which can be mounted in a way which simulates the expected spacecraft interface.

Initial tests at light levels still below those expected at Mercury show that the first baffle vane will reach a minimum of 84 °C and has a time constant of 0.4 h. The baffle does not reach equilibrium conditions over one orbital period. Dynamic tests (changing the angle of the mirror with time to simulate the motion of the MPO in its orbit) have just begun.

The thermal IR flux from the planet itself is also a major contributor to heat dissipation within the instrument when the spacecraft is above the dayside hemisphere. The Mercury thermal IR flux is simulated in the same chamber using a heating plate (Watlow Inc.). Two settings are available which can represent the solid angle subtended by Mercury at the spacecraft periherm and apoherm. The plate can be heated to 570 K and has been used to demonstrate the response of the electroformed nickel telescope to thermal cycling in Mercury orbit. The telescope has a time constant of 1.7 h. Of concern is that the secondary mirror can get considerably warmer than the primary. Given the need for an athermal design of the telescope, attention is now being placed on finding methods of reducing thermal gradients by using a high conductivity spider mount for the secondary. Note that the baffle ensures that the telescope should not be exposed to direct sunlight at any time during nominal operation.

7. Summary and concluding remarks

Following 18 months of activity, the design of the BELA has made significant progress. A baseline approach has been established and several critical items have been studied through detailed design and through prototype hardware development and test. A 10 Hz system has been baselined for a mass of 10.8 kg and a primary power consumption of 43.2 W. The estimated ranging accuracy from the experiment itself is 1.9 m although errors in the knowledge of the spacecraft pointing are expected to dominate the final error budget.

Overall, the altimetry performance of BELA is expected to be slightly inferior to that of MLA. However, for laser altimetry, the orbit of the MPO is far superior to that of the MESSENGER spacecraft. This will allow global mapping of the planet, rather than the more limited coverage offered by the MESSENGER spacecraft. Nonetheless, this comes at a price. The nadir-pointing configuration and the proximity to Mercury on a relatively short period orbit produce major challenges to the thermal design of the experiment. While the development of BELA is in an early phase, the approaches to thermal protection of the system (notably the reflective baffle) have already been shown to be feasible. The use of the telescope itself as a thermal enclosure has also been demonstrated. One outstanding issue is that tests are needed on the BEX and laser to investigate whether incoming sunlight can damage the transmitter system. Inevitably, the additional thermal hardware and the standalone nature of the instrument design are a major contributor to the higher mass than that of MLA.

While there remains much to do, the prospects for the successful development of the first European planetary laser altimeter appear good.

Acknowledgements

The authors wish to acknowledge major financial support from the Swiss Space Office (through PRODEX), the Max-Planck-Society, and the Deutsches Zentrum fuer Luft- und Raumfahrt. Further contributions have been made through grants from the Swiss National Fond, ESA supported technology studies, CNES and Spanish education ministry supported technology studies, and the Belgian Science Policy PRODEX program. The authors also wish to thank two anonymous referees for a series of extremely useful remarks.

References

Abshire, J.B., Sun, X., Afzal, R.S., 2000. Mars orbiter laser altimeter: receiver model and performance analysis. Appl. Opt. 39 (15), 2449–2460.

Anderson, J.M.M., Al Qatshan Abdel Sallam, 2001. Matched filtering-based estimation of ground elevation using laser altimetry. Proceedings of IEEE, pp. 2168–2175.

Brenner, A.C., Zwally, H.J., Bentley, C.R., Csathó, B.M., Harding, D.J., Hofton, M.A., Minster, J.-B., Roberts, L., Saba, J.L., Thomas, R.H., Donghui, Y., 2000. Derivation of range and range distributions from laser pulse waveform analysis for surface elevations, roughness, slope, and vegetation heights. Geoscience Laser Altimeter System (GLAS), Version 3:0, pp. 1–93.

Bufton, J.L., 1989. Laser altimetry measurements from aircraft and spacecraft. Proc. IEEE 77 (3), 463–477.

Cheng, A.F., Cole, T.D., Zuber, M.T., Smith, D.E., Guo, Y., Davidson, F., 2000. In-flight calibration of the near earth asteroid rendezvous laser rangefinder. Icarus 148, 572–586.

Cohen, E.R., Taylor, B.N., 1997. The fundamental physical constants. Phys. Today 50 (Part 2), BG7–BG11.

Cole, T.D., 1996. Spaceborne laser altimetry. Crit. Rev. 66, 383–405.

Gardner, C.S., 1982. Target signatures for laser altimeters: an analysis. Appl. Opt. 21 (3).

Gardner, C.S., 1992. Ranging performance of satellite laser altimeters. Proc. IEEE 30 (5), 1061–1072.

Gunderson, K., Thomas, N., Rohner, M., 2006. A laser altimeter model and its application to BELA, IEEE Trans. Geosci. Remote Sensing 44, 3308–3319.

Hofton, M.A., Minster, J.B., Blair, J.B., 2000. Decomposition of laser altimeter waveform. Proc. IEEE 38 (4), 1989–1996.

Kay, S.M., 1998. Fundamentals of Statistical Signal Processing: Estimation Theory. Prentice-Hall, Englewood Cliffs, NJ.

Kleinhans, W.A., 1976. Skew ray results for condensing light pipes and reflective baffles. Appl. Opt. 15, 2437–2439.

Krebs, D.J., Novo-Gradac, A.-M., Li, S.X., Lindauer, S.J., Afzal, R.S., Yu, A.W., 2005. Compact, passively Q-switched Nd: YAG laser for the MESSENGER mission to Mercury. Appl. Opt. 44 (9), 1715–1718.

Luthcke, S.B., Rowlands, D.D., McCarthy, J.J., Pavlis, D.E., Stoneking, E., 2000. Spaceborne laser-altimeter-pointing bias calibration from range residual analysis. J. Spacecraft Rockets 37 (3), 374–384.

Neumann, G.A., Rowlands, D.D., Lemoine, F.G., Smith, D.E., Zuber, M.T., 2001. Crossover analysis of mars orbiter laser altimeter data. J. Geophys. Res. 106 (E10), 753–768.

Ott, M.N., Proctor, M., Dodson, M., Macumurphy, S., Friedberg, P., 2003. Optical fiber cable assembly characterization for the Mercury laser altimeter. Proc. SPIE 5104, 96–106.

Ramos-Izquierdo, L., Bufton, J.L., Hayes, P., 1994. Optical system design and integration of the mars observer laser altimeter. Appl. Opt. 33 (3), 307–322.

Ramos-Izquierdo, L., Scott III, S., Schmidt, S., Britt, J., Mamakos, W., Trunzo, R., Cavanaugh, J., Miller, R., 2005. Optical system design and integration of the Mercury Laser Altimeter. Appl. Opt. 44, 1748–1760.

Robinson, M.S., Davies, M.E., Colvin, T.R., Edwards, K.E., 1997. A New Controlled Albedo Map of Mercury. Lunar and Planetary Sci. XXVIII, Abstract # 1128.

Seiferlin, K., Chakraborty, S., Gunderson, K., Fischer, J., Luethi, B.S., Piazza, D., Rieder, M., Sigrist, M., Thomas, N., Weigel, T. A lightweight reflective baffle for the BepiColombo Laser Altimeter: manufacture. Opt. Eng., in revision.

Sheppard, J.W., Kaufmann, M.A., 2005. A Bayesian approach to diagnosis and prognosis using built-in test. IEEE Trans. Instrum. Meas. 54 (3), 1003–1018.

Solomon, S.C., et al., 2001. The MESSENGER mission to Mercury: scientific objectives and implementation. Planet. Space Sci. 49, 1445.

Stavroudis, O.N., Foo, L.D., 1994. System of reflective telescope baffles. Opt. Eng. 33, 675–680.

Zuber, M.T., Smith, D.E., Solomon, S.C., Muhleman, D.O., Head, J.W., Garvin, J.B., Abshire, J.B., Bufton, J.L., 1992. J Geophys. Res 97 (E5), 7781–7797.